

A bright triggered twin-photon source in the solid state

A. Thoma¹, T. Heindel^{1,*}, A. Schlehahn¹, M. Gschrey¹, P. Schnauber¹, J.-H. Schulze¹,
A. Strittmatter¹, S. Rodt¹, A. Carmele², A. Knorr², and S. Reitzenstein¹

¹*Institut für Festkörperphysik, Technische Universität Berlin, 10623 Berlin, Germany*

²*Institut für Theoretische Physik, Technische Universität Berlin, 10623 Berlin, Germany*

*Corresponding author: tobias.heindel@tu-berlin.de

Abstract: A non-classical light source emitting pairs of identical photons represents a versatile resource of interdisciplinary importance with applications in quantum optics¹ and quantum biology². Emerging research fields, which benefit from such type of quantum light source, include quantum-optical spectroscopy³⁻⁵ or experiments on photoreceptor cells sensitive to photon statistics⁶. To date, photon twins have mostly been generated using parametric downconversion sources^{7,8}, relying on Poissonian number distributions, or atoms^{9,10}, exhibiting low emission rates. Here, we propose and experimentally demonstrate the efficient, triggered generation of photon twins using the energy-degenerate biexciton-exciton radiative cascade of a single semiconductor quantum dot. Deterministically integrated within a microlens, this nanostructure emits highly-correlated photon pairs, degenerate in energy and polarization, at a rate of up to (2.8 ± 0.4) MHz. Two-photon interference experiments reveal a significant degree of indistinguishability of both photons, and thus further prove that our source resembles a two-photon Fock-state $|2\rangle$.

To realize an integrated light source capable of emitting an N-photon Fock-state $|N\rangle$ is a fascinating, yet equally challenging task at the heart of quantum optics^{1,11,12}. Integrated schemes using parametric downconversion for the generation of photon twins have been demonstrated⁸, but still suffer from low efficiencies. Semiconductor quantum dots (QDs) turned out to be excellent quantum emitters¹³⁻¹⁵, which can produce close to ideal single-photon states with high efficiency under optical¹⁶⁻¹⁸ and electrical¹⁹ excitation. Typical photon-pair experiments exploiting the biexciton-exciton radiative cascade in QDs²¹ aim at the generation of entanglement^{20,21}. These experiments entirely relied on pairs of photons with different energies, which results from the fact that the biexciton state typically reveals a finite binding energy $E_{\text{bin}} \sim 1$ meV with respect to the case of two unbound excitons. The exciton state, on the other hand, is usually characterized by a fine structure splitting $\Delta E_{\text{FSS}} \sim 10$ μeV , which is small compared to E_{bin} . This leads to doublets of orthogonally linearly polarized emission lines for exciton and biexciton. Hence, the energy scales E_{bin} and ΔE_{FSS} set the requirements for the generation of pairs of identical photons by the biexciton-exciton radiative cascade.

In this work, we selected a QD fulfilling the condition $\Delta E_{\text{FSS}} = E_{\text{bin}}$ to demonstrate the triggered generation of photon-twins (cf. Fig. 1a). Here, one decay path of the XX-X radiative cascade reveals the emission of photon-twins – a light state constituted of two photons with identical emission energy and polarization. The QD is deterministically integrated within a monolithic microlens (cf. Fig. 1b) for enhanced photon collection efficiency²² (see Supplemental Material). Figure 1c shows photoluminescence spectra of the QD's emission under above-bandgap ($\lambda = 850$ nm) continuous wave excitation for linear-horizontal (H) and -vertical (V) polarization. In case of V-polarization a doublet centered at 1.33047 eV is observed, where the

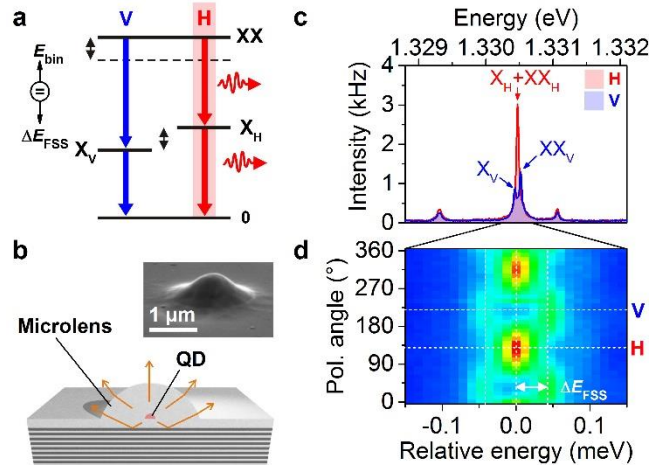


Figure 1: Concept of a deterministically integrated twin-photon source. (a) Energy level scheme of a radiative cascade involving the biexciton- (XX), exciton- (X) and ground- (0) state. In case of $\Delta E_{\text{FSS}} = E_{\text{bin}}$ the exciton fine structure splitting ΔE_{FSS} equals the biexciton binding energy E_{bin} and the photon pairs of one decay path exhibit identical energy and polarization. (b) Illustration of our solid-state based quantum light source constituted of a single quantum dot (QD) deterministically integrated within a monolithic microlens. The microlens design in combination with a lower distributed-Bragg reflector allows for an enhanced photon collection efficiency of photons emitted by the QD. Inset: Scanning electron microscopy image of a microlens. (c) Spectrally resolved photoluminescence of a single-QD microlens in linear-horizontal (H) and -vertical (V) polarization. For H-polarization the superimposed emission of exciton and biexciton leads to an increased emission intensity compared to V-polarization. (d) Polarization-resolved emission spectra in a close up with relative energy scale. A quantitative analysis reveals $\Delta E_{\text{FSS}} = E_{\text{bin}} = (51 \pm 6) \mu\text{eV}$. By selecting the H-polarized decay channel photon-twins can be extracted.

low- and high-energy component can be attributed to the excitonic (X_v) and biexcitonic (XX_v) emission, respectively (cf. Fig. 1a). Switching to H-polarization, a single, intense emission line can be observed at 1.33047 eV. This behavior is analyzed in more detail in Figure 1d, depicting a polarization-resolved map of photoluminescence spectra. Exciton and biexciton exhibit a sinusoidal shift in energy with opposite phase, however, close to H polarization their emission becomes superimposed, resulting in a distinct maximum of the emission intensity. A quantitative analysis of the spectra from Figure 1d yields $\Delta E_{\text{FSS}} = E_{\text{bin}} = (51 \pm 6) \mu\text{eV}$ (see Supplemental Material).

The dynamics of this unique four-level system were studied via polarization-resolved photon-correlation measurements²³. First, we address the correlations of the V-polarized cascade channel. In this case X and XX photons are energetically separable using two spectrometers (cf. schematic in Fig. 2a). Figure 2a displays the obtained cross-correlation coincidence histogram $g^{(2)}_{\text{cross}}(\tau)$, where XX-photons started and X-photons stopped the measurement. An asymmetric bunching effect is observed for positive delay times τ , owing to the cascaded emission of photon-pairs within the same decay channel²³⁻²⁵. Next, the photon correlations within the H-polarized decay channel are investigated. Here, exciton and biexciton photons are energetically degenerate and temporal correlations can be probed via photon auto-correlation measurements using a single spectrometer (cf. schematic in Fig. 2b). The corresponding coincidence histogram reveals a prominent bunching signature at zero delay and - due to the absence of time-ordering of the detected photons - a symmetric behavior in τ . The pronounced bunching indicates a high degree of two-photon correlations, which supports that this unique XX-X radiative cascade serves as a source of photon twins. Our experimental observations agree quantitatively with a theoretical model (solid curves) based on a four-level rate equation approach considering the experimental configurations (see Supplemental Material).

Interestingly, the bunching in auto-correlation is clearly lower compared to cross-correlation (cf. Fig. 2). This can be explained by considering the respective two-photon correlations, relevant to the corresponding measurement configuration.

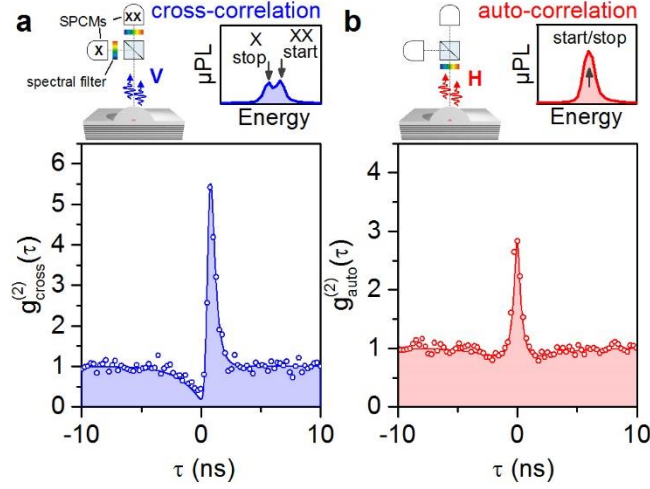


Figure 2: Polarization-resolved photon-correlations of photon pairs emitted by the quantum dot microlens under continuous wave excitation. (a) Photon cross-correlation histogram $g_{\text{cross}}^{(2)}(\tau)$ for the V-polarized decay channel, where biexciton and exciton emission are spectrally separated (cf. schematic of experiment and spectrum). The strong bunching signature at $\tau > 0$ in combination with an antibunching at $\tau < 0$ proves the cascaded emission of XX-X photon pairs. (b) Photon auto-correlation histogram $g_{\text{auto}}^{(2)}(\tau)$ for the H-polarized decay channel of the XX-X cascade, where biexciton and exciton emission is superimposed (cf. schematic). The pronounced bunching at $\tau = 0$ of $g_{\text{auto}}^{(2)}(0) = 2.85$ indicates a high degree of two-photon correlations, due to the emission of photon twins. Solid curves in both panels are theoretical simulations based on a four-level master equation approach accounting for the experimental conditions.

In case of the cross-correlation, each start- and stop-trigger of the coincidence measurement can be attributed to the distinct detection of one XX and one X photon. The corresponding observable of this cross-correlation measurement can be expressed (for $\tau \geq 0$) by $g_{\text{cross}}^{(2)} = g_{\text{XX} \rightarrow \text{X}}^{(2)}$. In case of the auto-correlation measurement on the degenerate H-polarized decay path, XX and X photons can be detected at both detectors. Thus the distinct time-order is lost and the correlation $g_{\text{XX} \rightarrow \text{X}}^{(2)}$ from above is superimposed by the time-inverted correlation $g_{\text{X} \rightarrow \text{XX}}^{(2)}$. Additionally, also the “true” auto-correlations, $g_{\text{X} \rightarrow \text{X}}^{(2)}$ and $g_{\text{XX} \rightarrow \text{XX}}^{(2)}$, of exciton and biexciton, respectively, have to be taken into account. The complete two-photon correlation $g_{\text{auto}}^{(2)}$ for H-polarization thus reads ($\tau \geq 0$):

$$g_{\text{auto}}^{(2)} = \alpha g_{\text{XX} \rightarrow \text{X}}^{(2)} + \beta g_{\text{X} \rightarrow \text{XX}}^{(2)} + \gamma g_{\text{X} \rightarrow \text{X}}^{(2)} + \delta g_{\text{XX} \rightarrow \text{XX}}^{(2)}. \quad (1)$$

Assuming that the probability to observe a given correlation in equation (1) is equally distributed yields $\alpha = \beta = \gamma = \delta \equiv 1/4$. Hence, by comparing the measured cross- and auto-correlation traces, one obtains information about the efficiency of the twin-photon source in terms of the probability to find a XX-X photon pair per excitation. In particular, we observe a preferred twin-photon emission if the condition $g_{\text{auto}}^{(2)}(0) > 1/4 \times g_{\text{cross}}^{(2)}(0)$ is fulfilled. Consequently, we evaluated the performance of our twin-photon source in terms of its efficiency by conducting excitation power dependent measurements. Figure 3a displays the excitation power dependencies of the integrated intensities of XX and X emission (extracted in V-polarization). The corresponding bunching values extracted from the auto- and cross-correlation traces (cf. Fig. 3b, inset) reveal a monotonous drop with increasing excitation. This behavior, typically observed in excitation-power dependent cross-correlation measurements^{26,27}, is a consequence of the increasing population of the X state and does not carry information on the probability to generate a photon pair. However, the decrease of the bunching for photon-twins (auto-correlation) is less pronounced compared to the distinguishable XX-X photon-pairs (cross-correlation), which indicates a change in the generation efficiency of photon twins in the degenerate cascade channel. The emission rate of photon-twins into the first lens can be extracted from

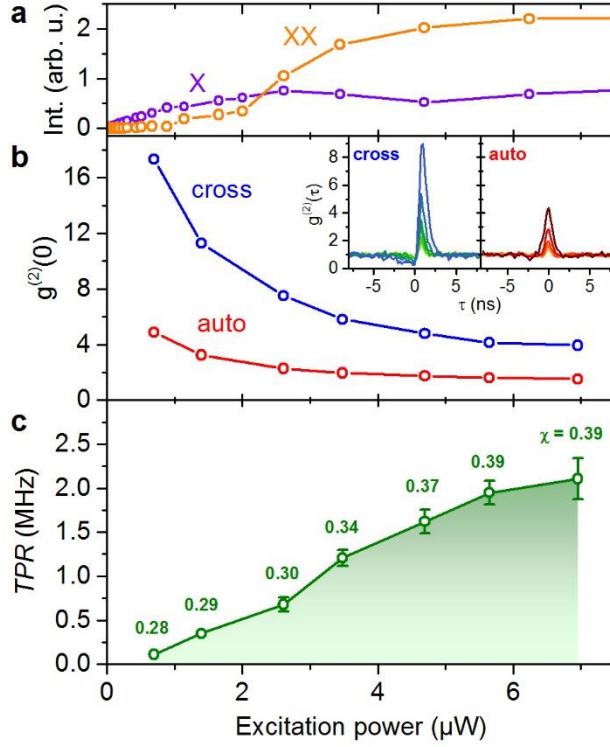


Figure 3: Excitation power dependence of twin-photon generation. (a) Integrated intensities of exciton and biexciton emission extracted for the V-polarized decay channel. The emission intensities of X and XX saturate at excitation powers of about 2 μW and 6 μW , respectively. (b) Bunching values $g^{(2)}(0)$ for auto- and cross-correlation resulting from a theoretical fit to the experimental data shown in the inset (taking into account the setup’s timing resolution). (c) Excitation power dependence of the twin-photon emission rate (TPR) into the first lens of the setup. The TPR is assumed proportional to the ratio $\chi = g^{(2)}_{\text{auto}}(0)/g^{(2)}_{\text{cross}}(0)$ calculated from the bunching values in (c).

the combined single-photon detection rates n_{SPCMs} in H-polarization, by taking into account the setup collection efficiency ϵ (see Supplemental Material), and considering the bunching ratio $\chi = g^{(2)}_{\text{auto}}(0)/g^{(2)}_{\text{cross}}(0)$. Interpreting χ as the probability to generate a photon twin per excitation (cf. discussion of equation (1)), the corresponding twin-photon rate TPR can be expressed via $TPR = \frac{1}{2} \times \chi \times n_{\text{SPCMs}} \times \epsilon^{-1}$, where the factor $\frac{1}{2}$ takes into account that in 50% of all cases a XX-X pair was split at the HBT beam splitter leading to two detection events. Figure 3c presents the deduced twin-photon rate TPR and the respective ratio χ calculated from Fig. 3b. With increasing excitation the twin-photon generation efficiency monotonously rises and reaches a maximum value of $\chi = 0.39 \pm 0.03$. At this working point the TPR saturates at a maximum value of (2.1 ± 0.2) MHz. This represents more than an order of magnitude (factor 42) improvement compared to photon twins generated with atoms¹⁰.

To operate our quantum light source as two-photon gun, we used pulsed above-bandgap excitation. Figure 4a displays the auto-correlation histogram of the energy-degenerate decay channel (H-polarization), which proves the predominance of two-photon correlations also under pulsed excitation. At saturation power (1 μW), we observe a triggered TPR of (2.8 ± 0.4) MHz, resulting in a twin-photon collection efficiency per pulse of (3.5 ± 0.5) %. This contrasts favorably to SPDC sources with efficiencies of 0.4 % at reasonable, heralded antibunching values ($g^{(2)}(0) \sim 0.01$)¹⁷. Utilizing anti-reflection coatings²⁸ or a bottom gold mirror²², we expect further improved twin-photon collection efficiencies of 10–16 % (assuming $\chi = 0.39$ and photon extraction efficiencies of 50–80%).

Furthermore, we tested the indistinguishability of both photons emitted within the H-polarized decay channel, by means of Hong-Ou-Mandel (HOM) -type two-photon interference (TPI) experiments (see Supplemental Material) under pulsed

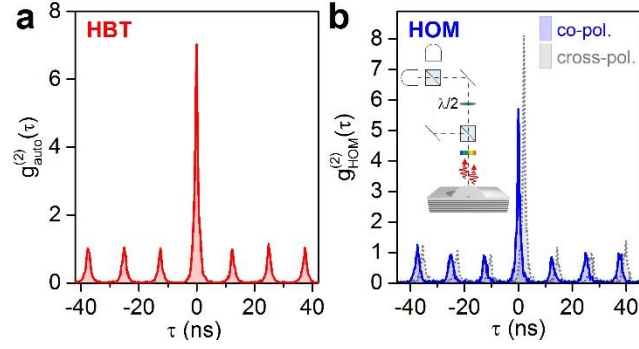


Figure 4: Triggered generation of photon twins (H-polarization). (a) Measured photon auto-correlation histogram $g_{\text{auto}}^{(2)}(\tau)$ of photon-twins under pulsed above-band excitation at low excitation power ($P = 87$ nW). A bunching of $g_{\text{auto}}^{(2)}(0) = A_0/A = 5.1$ is observed, where A_0 and A correspond to the zero-delay peak and the peaks at finite τ . (b) Hong-Ou-Mandel (HOM) two-photon interference experiment using photon-twins under pulsed p -shell excitation. Measured histograms of $g_{\text{HOM}}^{(2)}(\tau)$ for co-polarized (solid line) and cross-polarized (dashed line) configuration using a symmetric Mach-Zehnder interferometer (data in cross-polarization shifted by +2 ns for clarity).

excitation into the QD's p -shell ($\lambda = 904.5$ nm). Triggered photon-twins are sent into a symmetric Mach-Zehnder interferometer, where a $\lambda/2$ -waveplate within one interferometer arm allows for switching between co- and cross-polarized measurement configuration (cf. Fig. 4b, illustration). Figure 4b presents the TPI histograms $g_{\text{HOM}}^{(2)}(\tau)$ for both measurement configurations. A clear reduction in coincidences is observed at $\tau = 0$ for co-polarized measurement configuration, proving the interference of photons emitted by the cascade. Considering the bunching values $g_{\parallel}^{(2)}(0)$ and $g_{\perp}^{(2)}(0)$ extracted from the coincidence peak-area ratios yields a visibility of two-photon interference of $V = \frac{g_{\perp}^{(2)}(0) - g_{\parallel}^{(2)}(0)}{g_{\perp}^{(2)}(0) \times 1/2} = (55.7 \pm 9.2) \%$ (see Supplemental Material for details). Limiting factors for the observed indistinguishability are discussed in the Supplemental Material and can be encountered by applying strictly resonant excitation schemes via simultaneous one- and two-photon excitation or exploiting cavity effects.

In conclusion, the integrated QD-based twin-photon source presented in this work is an attractive type of quantum light source. Efficient, triggered generation of photon pairs with same energy and polarization becomes possible by utilizing a biexciton-exciton radiative cascade, where the biexciton binding energy equals the bright exciton's fine structure splitting. We proved that the emission of our source resembles a two-photon Fock-state $|2\rangle$, which is very attractive novel quantum optics experiments, such as the excitation of quantum-degenerate quasi-particle states³. Combining our approach with readily available technologies, such as electrical control²⁹ and piezo-tuning³⁰, the realization of practical, user-friendly twin-photon sources is within reach.

Acknowledgments: We acknowledge support from the German Research Foundation (DFG) via the SFB 787 "Semiconductor Nanophotonics: Materials, Models, Devices" and Grant RE2974/9-1 as well as the German Federal Ministry of Education and Research (BMBF) via the VIP-project QSOURCE (Grant No. 03V0630). A. C. gratefully acknowledges support from the SFB 910: "Control of self-organizing nonlinear systems". The authors gratefully acknowledge sample processing by R. Schmidt and technical assistance by M. Schlösinger.

Supplemental Material

Sample: The QD sample utilized for our experiments was grown by metal-organic chemical vapor deposition (MOCVD) on GaAs (001) substrate. Self-organized InGaAs QDs are deposited above a lower distributed Bragg reflector (DBR) constituted of 23 alternating $\lambda/4$ -thick bi-layers of AlGaAs/GaAs. On top of the QD layer, a 400 nm-thick GaAs capping layer provides the material for the subsequent microlens fabrication. Deterministic single-QD microlenses were processed via 3D in-situ electron-beam lithography based on cathodoluminescence (CL) spectroscopy²². Shallow hemispheric-section-type microlenses with heights of 400 nm and base widths of 2.4 μm have been chosen, allowing for a photon extraction efficiency of up to 29 %³¹.

Experimental setup: For the micro-photoluminescence (μPL) investigations, the sample is mounted onto the cold-finger of a liquid-Helium-flow cryostat and held at a temperature of $T = 6$ K. The QD microlens is optically excited using a tunable Ti:sapphire laser operating in continuous wave or pulsed picosecond mode ($f = 80$ MHz). Photoluminescence is collected via a microscope objective with a numerical aperture (NA) of 0.4 serving as first lens of the detection system. The μPL signal is spectrally analyzed using a grating spectrometer with an attached charge-coupled device camera enabling a spectral resolution of 25 μeV . Two-photon emission of the deterministic QD microlens is further studied via polarization-resolved photon-correlation experiments. In case of photon auto-correlation measurements, the superimposed exciton and biexciton emission (H-polarization) is spectrally selected using a single monochromator and analyzed using a fiber-based Hanbury-Brown and Twiss (HBT) setup containing a 50:50 multi-mode beamsplitter. For photon cross-correlation measurements the spectrally distinguishable exciton and biexciton emission (V-polarization) is spatially separated using two monochromators. In both cases (auto- and cross-correlation), coincidence measurements are performed using two fiber-coupled Silicon-based single-photon counting modules (SPCM) with an overall timing resolution of 350 ps in combination with time-correlated single-photon counting electronics with 4 ps time-bin width. In order to determine the efficiency of our twin-photon source from the detected count rates at the SPCMs, we measured the collection efficiency ε of our experimental setup to be (0.95 ± 0.05) % following ref. 22. The indistinguishability of photons from the emitted biexciton-exciton pair is studied by means of Hong-Ou-Mandel (HOM)-type two-photon interference measurements via a Mach-Zehnder interferometer based on polarization maintaining fibers. A $\lambda/2$ -waveplate allows to switch the polarization of photons in one of the interferometer arms, either being co- or cross-polarized with respect to photons in the other arm. The Mach-Zehnder interferometer in this work - in contrast to e.g. ref. 22 - was chosen symmetric with respect to the arm length, taking account for a negligible temporal delay between photon-twins.

Two-photon interference visibility: To extract the two-photon interference visibility from measured $g_{\text{HOM}}^{(2)}(\tau)$ traces, we first determined the peak area ratio $g_{\text{HOM}}^{(2)}(0) = A_0/A$, where A_0 corresponds to the area of the zero-delay peak and A is the mean area of the peaks at $\tau \neq 0$. Even in the case of perfect indistinguishability of X and XX photons, one expects a finite contrast between the measurements in co- and cross-polarized configuration according to $g_{\text{HOM},\parallel}^{(2)}(0) = \frac{1}{2} g_{\text{HOM},\perp}^{(2)}(0)$. The respective coincidences in co-polarized configuration arise from the fact, that in 50 % of all cases both photons of the exciton-biexciton pair will take the same path within the interferometer. Hence, they enter the second beam splitter at the same entrance port and

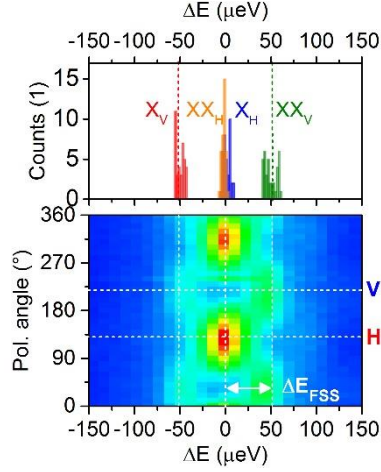


Fig. S1: Quantitative analysis of the polarization resolved spectra. The histogram (upper panel) shows the relative spectral positions of the four H- and V-polarized exciton (X) and biexciton (XX) components extracted from a total of 36 spectra displayed in the lower panel.

thus cannot lead to two-photon interference. Consequently, the two-photon interference visibility has to be renormalized by a

factor of 2 compared to the standard formula³² according to $V = \frac{g_{\perp}^{(2)}(0) - g_{\parallel}^{(2)}(0)}{g_{\perp}^{(2)}(0) \times 1/2}$.

Polarization-resolved measurements: In order to quantitatively determine the fine-structure splitting ΔE_{FSS} of the QD's bright exciton states, we applied fits to the QD-emission spectra shown in Figure 1d of the main article. We used four Lorentzian profiles corresponding to the linearly polarized emission lines X_{H} and X_{V} as well as XX_{H} and XX_{V} of the exciton- and biexciton-state, respectively. For carrying out the fits we made the following assumptions: Firstly, both excitonic and both biexcitonic components are assumed to have the same spectral linewidth γ : $\gamma_{X,\text{H}} = \gamma_{X,\text{V}}$ and $\gamma_{XX,\text{H}} = \gamma_{XX,\text{V}}$. Secondly, the energetic splitting of the excitonic components equals the splitting of the biexcitonic components, which accounts for the fact that only the exciton state reveals a fine-structure splitting: $\Delta E_{X,\text{H-V}} = \Delta E_{XX,\text{H-V}} = \Delta E_{\text{FSS}}$. Additionally, the ratio of the integrated intensities of exciton and biexciton is the same for both polarizations: $I_{X,\text{H}}/I_{XX,\text{H}} = I_{X,\text{V}}/I_{XX,\text{V}}$, which corresponds to an unpolarized radiative cascade. The resulting relative spectral positions of the emission lines extracted from the fits to a total of 36 spectra are depicted in Figure S1 in a histogram (upper panel) together with the original polarization- and energy-resolved contour plot (lower panel). A statistical analysis reveals mean relative spectral positions of $\Delta E_{X,\text{H}} = (+1.9 \pm 3.7) \mu\text{eV}$ and $\Delta E_{XX,\text{H}} = (-1.9 \pm 2.1) \mu\text{eV}$ for the H-polarized exciton and biexciton component, respectively, which coincide within their standard deviation. Hence, the photon-twins emitted in the H-polarized decay channel can be considered degenerate in energy and polarization. Further, taking into account the relative spectral positions of $\Delta E_{X,\text{V}}$ and $\Delta E_{XX,\text{V}}$ for the V-polarized decay channel, we can extract a fine-structure splitting of $\Delta E_{\text{FSS}} = (51 \pm 6) \mu\text{eV}$.

Rate equation model: For a theoretical description of our twin-photon source, we model the quantum dot as a four-level system constituted of a ground-state $|G\rangle$, two bright exciton states $|H\rangle$ and $|V\rangle$, and a biexciton state $|B\rangle$. The dynamics of the excitonic levels can thus be expressed by the following rate equations for the state-occupation probabilities ρ :

$$\frac{d}{dt} \rho_{BB} = -2\Gamma_B \rho_{BB} + P_B (\rho_{VV} + \rho_{HH})$$

$$\begin{aligned}\frac{d}{dt}\rho_{HH} &= -\Gamma_X\rho_{HH} + \Gamma_B\rho_{BB} - P_B\rho_{BB} + P_X\rho_{GG} \\ \frac{d}{dt}\rho_{VV} &= -\Gamma_X\rho_{VV} + \Gamma_B\rho_{BB} - P_B\rho_{BB} + P_X\rho_{GG} \\ \frac{d}{dt}\rho_{GG} &= -2P_X\rho_{GG} + \Gamma_X(\rho_{HH} + \rho_{VV}),\end{aligned}$$

where Γ_B (P_B) and Γ_X (P_X) correspond to the decay (pump) rates of the biexciton state and both exciton states. To connect the dynamics to the measurement, we assume within the far field approximation that the photon detection events are proportional to dipole excitations: $c_i^\dagger \equiv \sigma_{Bi} + \sigma_{iG}$, with $i = H, V$. Using this relation and the rate equations above, we can calculate the two-photon correlations $g^{(2)}(\tau \geq 0)$ in Formula (1) of the main text using the quantum regression theorem¹:

$$\begin{aligned}g_{XX \rightarrow X}^{(2)} &= \frac{\langle \sigma_{BH}(0)\sigma_{HG}(\tau)\sigma_{GH}(\tau)\sigma_{HB}(0) \rangle}{\langle \sigma_{BH}\sigma_{HB} \rangle \langle \sigma_{HG}\sigma_{GH} \rangle} \\ &= \frac{Na}{4\alpha P^3 \Gamma_B} (\beta_1 + \beta_2 e^{-(\Gamma_X + P)\tau} + \beta_3 e^{-(0.5\Gamma_X + \Gamma_B + 1.5P - 0.5\sqrt{\alpha})\tau} + \beta_4 e^{-(0.5\Gamma_X + \Gamma_B + 1.5P + 0.5\sqrt{\alpha})\tau})\end{aligned}$$

$$\begin{aligned}g_{X \rightarrow XX}^{(2)} &= \frac{\langle \sigma_{HG}(0)\sigma_{BH}(\tau)\sigma_{HB}(\tau)\sigma_{GH}(0) \rangle}{\langle \sigma_{BH}\sigma_{HB} \rangle \langle \sigma_{HG}\sigma_{GH} \rangle} \\ &= \frac{e^{-(\Gamma_X + 2\Gamma_B + 3P + \sqrt{\alpha})\frac{\tau}{2}}}{2} \left(\frac{(1 - e^{\tau\sqrt{\alpha}})(\Gamma_X + 2\Gamma_B + 3P)}{\sqrt{\alpha}} - 1 - e^{\tau\sqrt{\alpha}} \right) + 1\end{aligned}$$

$$\begin{aligned}g_{X \rightarrow X}^{(2)} &= \frac{\langle \sigma_{HG}(0)\sigma_{HG}(\tau)\sigma_{GH}(\tau)\sigma_{GH}(0) \rangle}{\langle \sigma_{HG}\sigma_{GH} \rangle^2} \\ &= \frac{e^{-(\Gamma_X + 2\Gamma_B + 3P + \sqrt{\alpha})\frac{\tau}{2}}}{2\Gamma_B\sqrt{\alpha}} \left(-\Gamma_B\sqrt{\alpha}(1 + e^{\tau\sqrt{\alpha}}) - (1 - e^{\tau\sqrt{\alpha}})((\Gamma_X - 2\Gamma_B)\Gamma_B + \Gamma_B P + P^2) \right) + 1\end{aligned}$$

$$\begin{aligned}g_{XX \rightarrow XX}^{(2)} &= \frac{\langle \sigma_{BH}(0)\sigma_{BH}(\tau)\sigma_{HB}(\tau)\sigma_{HB}(0) \rangle}{\langle \sigma_{BH}\sigma_{HB} \rangle^2} \\ &= \frac{e^{-(\Gamma_X + 2\Gamma_B + 3P + \sqrt{\alpha})\frac{\tau}{2}}}{2P\sqrt{\alpha}} \left((1 - e^{\tau\sqrt{\alpha}})(\Gamma_X + P)(-2\Gamma_B + P) - P\sqrt{\alpha}(1 + e^{\tau\sqrt{\alpha}}) \right) + 1\end{aligned}$$

The following abbreviations were introduced for clarity:

$$\begin{aligned}P &= P_X = P_B \\ N &= \Gamma_X\Gamma_B + 2P\Gamma_B + P^2 \\ \alpha &= (\Gamma_X - 2\Gamma_B)^2 + 6\Gamma_X P - 4\Gamma_B P + P^2 \\ \beta_1 &= 4\Gamma_B P \alpha \\ \beta_2 &= 2\alpha N\end{aligned}$$

$$\begin{aligned}
\beta_3 &= \Gamma_X^3 \Gamma_B - P^2 (2\Gamma_B - P) (-2\Gamma_B + P + \sqrt{\alpha}) + \Gamma_X^2 (-4\Gamma_B^2 + 6\Gamma_B + P^2 - \Gamma_B \sqrt{\alpha}) \\
&\quad + \Gamma_X (4\Gamma_B^3 + P^2 (6P - \sqrt{\alpha}) + 2\Gamma_B^2 (-2P + \sqrt{\alpha}) - 3\Gamma_B P (P + \sqrt{\alpha})) \\
\beta_4 &= \Gamma_X^3 \Gamma_B + P^2 (2\Gamma_B - P) (2\Gamma_B - P + \sqrt{\alpha}) + \Gamma_X^2 (-4\Gamma_B^2 + 6\Gamma_B P + P^2 + \Gamma_B \sqrt{\alpha}) \\
&\quad + \Gamma_X (4\Gamma_B^3 + P^2 (6P + \sqrt{\alpha}) + 2\Gamma_B^2 (-2P + \sqrt{\alpha}) + 3\Gamma_B P (-P + \sqrt{\alpha})) \\
Z &= 4\alpha N \\
\langle \sigma_{BH} \sigma_{HB} \rangle &= \frac{P^2}{N} = a \\
\langle \sigma_{HG} \sigma_{GH} \rangle &= \frac{P\Gamma_B}{N}
\end{aligned}$$

In case of the photon cross-correlation on spectrally separable biexciton-exciton photons (see main article, Fig. 2a), the correlation $g_{X \rightarrow XX}^{(2)}$ and $g_{XX \rightarrow X}^{(2)}$ have to be taken into account for negative and positive temporal delay τ . In case of the photon auto-correlation on spectrally degenerate biexciton-exciton photons (see main article, Fig. 2b), all four correlations from above have to be considered. In order to account for the timing resolution of the experimental setup, the theoretical correlation functions are convoluted with a Gaussian of 350 ps full-width at half maximum. Finally, the experimentally determined two-photon correlations in Figure 2 and 3 are fitted using the derived model.

Indistinguishability of photon twins: For the two-photon interference visibility of photon twins observed in our experiment (cf. Fig. 4b) the following contributions can be considered: Firstly, pure dephasing in terms of an inhomogeneous spectral broadening of the quantum dot emission results in a reduced wavepacket overlap¹⁴. A method to measure the corresponding time scale of spectral diffusion has been introduced very recently³³ and can be encountered in future by optimized QD growth¹⁶ or electrically controlled microlens devices²⁹ to reduce electric field noise¹⁷. Secondly, in the case of interfering photons from the XX-X radiative cascade, exciton and biexciton state have different radiative lifetimes, independently measured to be $\tau_X = (1.77 \pm 0.05)$ ns and $\tau_{XX} = (0.95 \pm 0.08)$ ns, and the biexciton's radiative decay introduces an additional time jitter between the X and XX photons. This issue can be encountered in future by utilizing cavity effects to reduce the radiative lifetime via the Purcell-effect²¹ or to induce spontaneous two-photon emission³⁴. Additionally, strictly resonant excitation can be applied in future, which eliminates any residual time jitter due to charge carrier relaxation. In this case, resonant excitation would be particular interesting, as the laser coherently drives two quantum emitters: The biexciton state via two-photon excitation²¹ and the exciton state via one-photon excitation, at which the X_H -level is congruent with the virtual intermediate level of the two-photon excitation process.

References:

1. R. Loudon, *The quantum theory of light* (Oxford University Press, USA, 1983).
2. P. Ball, *Nature* **474**, 272-274 (2011).
3. M. Kira, & S. W. Koch, *Phys. Rev. A* **73**, 013813 (2006).
4. A. Carmele et al., *Phys. Rev. B* **79**, 035316 (2009).
5. M. Strauß et al., *Phys. Rev. B* **93**, 241306 (2016)

6. N. Sim et al., *Phys. Rev. Lett.* **109**, 113601 (2012).
7. P. G. Kwiat et al., *Phys. Rev. Lett.* **75**, 4337-4341 (1995).
8. R. Horn et al., *Phys. Rev. Lett.* **108**, 153605 (2012).
9. P. Bertet et al., *Phys. Rev. Lett.* **88**, 143601 (2002).
10. J. K. Thompson et al., *Science* **313**, 74-77 (2006).
11. C. S. Muñoz et al., *Nature Photon.* **8**, 550 (2014).
12. F. Jahnke et al., *Nature Commun.* **7**, 11540 (2016).
13. P. Michler et al., *Science* **290**, 2282 (2000).
14. C. Santori et al., *Nature* **419**, 594-597 (2002).
15. C. H. H. Schulte et al., *Nature* **525**, 222 (2015).
16. H. Wang et al., *Phys. Rev. Lett.* **116**, 213601 (2016).
17. N. Somaschi et al., *Nat. Photon.* **10**, 340-345 (2016).
18. S. Unsleber et al., *Opt. Express* **24**, 8539 (2016).
19. A. Schlehahn et al., *APL Photonics* **1**, 011301 (2016).
20. N. Akopian et al., *Phys. Rev. Lett.* **96**, 130501 (2006).
21. M. Müller et al., *Nature Photon.* **8**, 224-228 (2014).
22. M. Gschrey et al., *Nat. Commun.* **6**, 7662 (2015).
23. D. V. Regelman et al., *Phys. Rev. Lett.* **87**, 257401 (2001).
24. E. Dekel et al., *Phys. Rev. B* **62**, 11038 (2000).
25. A. Kiraz et al., *Phys. Rev. B* **65**, 161303 (2002).
26. T. Kuroda et al., *Phys. Rev. B* **79**, 035330 (2009).
27. G. Callsen et al., *Phys. Rev. B* **87**, 245314 (2013).
28. P. Schnauber et al., *Technologies* **4**, 1 (2016).
29. A. Schlehahn et al., *Appl. Phys. Lett.* **108**, 021104 (2016).
30. F. Ding et al., *Phys. Rev. Lett.* **104**, 067405 (2010).
31. A. Schlehahn et al., *Appl. Phys. Lett.* **107**, 041105 (2015).
32. R. B. Patel et al., *Phys. Rev. Lett.* **100**, 207405 (2008).
33. A. Thoma et al., *Phys. Rev. Lett.* **116**, 033601 (2016).
34. Y. Ota et al., *Phys. Rev. Lett.* **107**, 2033602 (2011).